

Statistical characteristics of midlatitude ionospheric F-region backscatter observed by the SuperDARN Jiamusi radar

wei wang¹, Jiaojiao Zhang², Chi Wang², Junjie Chen³, Tong Dang⁴, and Jiuhou Lei⁴

¹University of the Chinese Academy of Sciences, Beijing, China

²State Key Laboratory of Space Weather, National Space Science Center (NSSC), Chinese Academy of Sciences, Beijing, China

³University of the Chinese Academy of Sciences

⁴University of Science and Technology of China

November 23, 2022

Abstract

The Jiamusi (JME) radar is the first high-frequency coherent scatter radar independently developed in China. In this study, we investigate the statistical characteristics of the occurrence rate of F-region ionospheric irregularities between 40°N and 65°N geomagnetic latitude by using the Jiamusi radar data from March 2018 to November 2019. Diurnal and seasonal variations in scattering echoes and their dependence on geomagnetic conditions are statistically investigated. It is shown that the local time of the peak echo occurrence rate varies depending on the season, i.e., approximately 20-22.5 magnetic local time (MLT) in summer, 17.5-20.5 MLT in equinox, and 16-17.5 MLT in winter, which is closely associated with the time of sunset. The echo occurrence rate also increases with the enhancement of the geomagnetic index. To further understand the mechanism of these features, we simulate the distribution of the gradient drift instability indicator ($(\nabla n \times \mathbf{V} E) / n$) by using the Thermosphere-Ionosphere-Electrodynamics General Circulation Model (TIEGCM). The analysis results indicate that the gradient drift instability is an important mechanism for irregularities in this region. Key points: 1. Diurnal and seasonal variations in the scatter occurrence rate and their dependence on Kp conditions are statistically analyzed. 2. The distribution of the gradient drift instability indicator ($(\nabla n \times \mathbf{V} E) / n$) is simulated by using the TIEGCM. 3. The gradient drift instability is an important mechanism for the high occurrence rate of echoes in the midlatitude region.

Statistical characteristics of midlatitude ionospheric F-region backscatter observed by the SuperDARN Jiamusi radar

Wei Wang^{1,2}, Jiaojiao Zhang^{1,2}, Chi Wang^{1,2}, Junjie Chen³, Tong Dang⁴, Jiuhou Lei⁴

¹University of the Chinese Academy of Sciences, Beijing, China

²State Key Laboratory of Space Weather, National Space Science Center (NSSC), Chinese Academy of Sciences, Beijing, China

³Department of Earth Sciences, the University of Hong Kong, Pokfulam, Hong Kong SAR, China

⁴CAS Key Laboratory of Geospace Environment, School of Earth and Space Sciences, University of Science and Technology of China, Hefei, China

Abstract: The Jiamusi (JME) radar is the first high-frequency coherent scatter radar independently developed in China. In this study, we investigate the statistical characteristics of the occurrence rate of F-region ionospheric irregularities between 40°N and 65°N geomagnetic latitude by using the Jiamusi radar data from March 2018 to November 2019. Diurnal and seasonal variations in scattering echoes and their dependence on geomagnetic conditions are statistically investigated. It is shown that the local time of the peak echo occurrence rate varies depending on the season, i.e., approximately 20-22.5 magnetic local time (MLT) in summer, 17.5-20.5 MLT in equinox, and 16-17.5 MLT in winter, which is closely associated with the time of sunset. The echo occurrence rate also increases with the enhancement of the geomagnetic index. To further understand the mechanism of these features, we simulate the distribution of the gradient drift instability indicator ($\nabla n \cdot \overline{V_E}/n$) by using the Thermosphere-Ionosphere-Electrodynamics General Circulation Model (TIEGCM). The analysis results indicate that the gradient drift instability is an important mechanism for irregularities in this region.

Key points:

1. Diurnal and seasonal variations in the scatter occurrence rate and their dependence on Kp conditions are statistically analyzed.
2. The distribution of the gradient drift instability indicator ($\nabla n \cdot \overline{V_E}/n$) is simulated by using the TIEGCM.
3. The gradient drift instability is an important mechanism for the high occurrence rate of echoes in the midlatitude region.

Correspondence to: Jiaojiao Zhang and Chi Wang,

jjzhang@spaceweather.ac.cn; cw@spaceweather.ac.cn

1. Introduction

The midlatitude ionosphere is an important region for the coupled magnetosphere-ionosphere-thermosphere system. The electric field generated by Rayleigh-Taylor (R-T) instability maps to the middle latitudes along the magnetic field lines, and the magnetotail/high latitude electric field [Blanc et al., 1977] also affects the emergence of midlatitude ionospheric irregularities.

Hosokawa et al. [2001] presented the statistical distributions of high frequency (HF) echoes at the subauroral region observed by six Northern Hemisphere SuperDARN radars. They found that the most prominent backscatter target of the SuperDARN radars is the scatter enhancement on the dusk side and thought that it corresponded to a plasma density depleted region, the midlatitude trough. They also found that this feature is most clearly observed around the summer and winter solstices. A subsequent study by Hosokawa et al. [2010] proposed an explanation of the formation of the scatter enhancement. They thought that the sunward plasma density gradient at the sunward edge of the midlatitude trough and an ambient poleward electric field are the dominant drivers of this phenomenon. Hu et al. [2013] presented the statistical characteristics of ionospheric backscatter observed by the SuperDARN Zhongshan radar. They found that in the Southern Hemisphere, the average power, line-of-sight velocity, spectral widths and occurrence rate were generally larger in winter than in summer. They also found that during geomagnetic quiet times, the peak echo occurrence rate appears on the day side, shifts toward the night side, and exhibits an obvious decrease with increasing Kp index.

The gradient density instability (GDI), also called $E \times B$ instability, has been generally considered to be one of the important mechanisms of ionospheric irregularity at midlatitudes [Keskinen and Ossakow, 1983]. In the ionospheric F region, the GDI can be stabilized when the ambient electric field, which generates the instability, has a modest component along the density gradient. At present, most of the research on the relationship between the occurrence rate distribution of irregularities in the ionospheric F region and GDI uses the electronic density gradient and plasma drift velocity or ionospheric electric field at the dusk side and dawn side ends of the midlatitude ionospheric trough (MIT). The distribution characteristics of the GDI at different magnetic local times and magnetic latitudes (MLAT) are still unclear, and the correlation between the GDI and the generation of irregularities in the F region of the midlatitude ionosphere needs further study.

The Super Dual Auroral Radar Network (SuperDARN) consists of several high-frequency coherent radars in both the Northern and Southern Hemispheres. The concept was developed to observe the characteristics of ionospheric convection through the detection of decameter-scale field-aligned ionospheric irregularities in the polar region [e.g., Greenwald et al., 1995]. However, during storms, the irregularity convection expands to the midlatitudes and may eventually extend beyond the field of view of these radars. Currently, SuperDARN has included more midlatitude

radars to improve large-scale observations of ionospheric irregularities and has more than 30 radars globally. The eleventh (the newest) SuperDARN midlatitude radar in the Northern Hemisphere was constructed in Jiamusi (46.8°N, 130.5°E), China. The location of the JME radar is approximately ten degrees lower than the midlatitude SuperDARN radars in North America. It can observe the region from 40°N to 65°N magnetic latitudes.

In this paper, we investigate the basic statistical characteristics of scattering echoes in the F region by using observations from the Jiamusi radar from March 2018 to November 2019. We study the diurnal and seasonal variations in the ionospheric echo occurrence rate and their dependence on geomagnetic (K_p) conditions. To clearly show the relationship between the occurrence rate of irregularities and the gradient drift instabilities, the TIEGCM is used to simulate the gradient density instability indicator ($\nabla n \cdot \vec{V}_E/n$) in this paper.

We give a brief introduction of the Jiamusi radar, the sources of the statistical dataset, the data processing method, the TEC data and the TIEGCM in Section 2. In the third section, the distribution of radar echo occurrence rates under different seasonal and geomagnetic conditions is shown. In the fourth section, we analyze the characteristics of these statistical results and combine them with the plasma drift velocity simulated by the TIEGCM and total electron content (TEC) observed by GNSS. A discussion and summary are presented in Sections 5 and 6, respectively.

2. Data and methods

2.1. Jiamusi radar

Figure 1 shows the fields of view of the SuperDARN radars in the Northern Hemisphere. The field of view of polar radars is marked in green, the rest of the high latitude radars are marked in blue, and the midlatitude radars are uniformly marked in red. The field of view of the Jiamusi radar is marked by a dotted line. It is located at 46.8°N and 130.5°E in geographic coordinates, (41.8°N and 155.1°W in geomagnetic coordinate), and has been established and in operation since 2018. This radar comprises the main array of 16 twin-terminated folded dipole antennas. It operates in the frequency band from 8-20 MHz with both transmitting and receiving capabilities, and has a 4 antennas interferometer array 100 m apart from the main array. The antennas can receive HF backscatter echoes from a slant range of 180-3000 km and from different ionospheric regions, including the D region, E region, and F region, depending on the number of gates (with a range resolution of 45 km). The boresight of the Jiamusi radar points 44° apart from the geographic north. Zhang et al. [2020] and Wang et al. [2021] validated the data by comparing the data from the Jiamusi radar and Hokkaido East radar during storm and quiet geomagnetic conditions.

Most SuperDARN radar echoes are 0.5 hop, 1 hop, 1.5 hop, and 2 hop propagations [Ribeiro A.J. et al., 2011]. When the direction of propagation of the decameter-scale irregularities is

perpendicular to the geomagnetic field, the radar picks up the echo signals, which is the principle of a 0.5 hop echo. The 1 hop signals of the ground and sea echoes are refracted by the ionosphere and picked up by the radar. In contrast, 1.5 and 2.0 hop signals bounce off the ground, re-enter the ionosphere, and then bounce back to the radar. The 1.5 hop signals are ionospheric scattering echoes, while the 2 hop signals are ground and sea echoes. This principle allows the radar to detect echoes over long distances (0-3000 km).

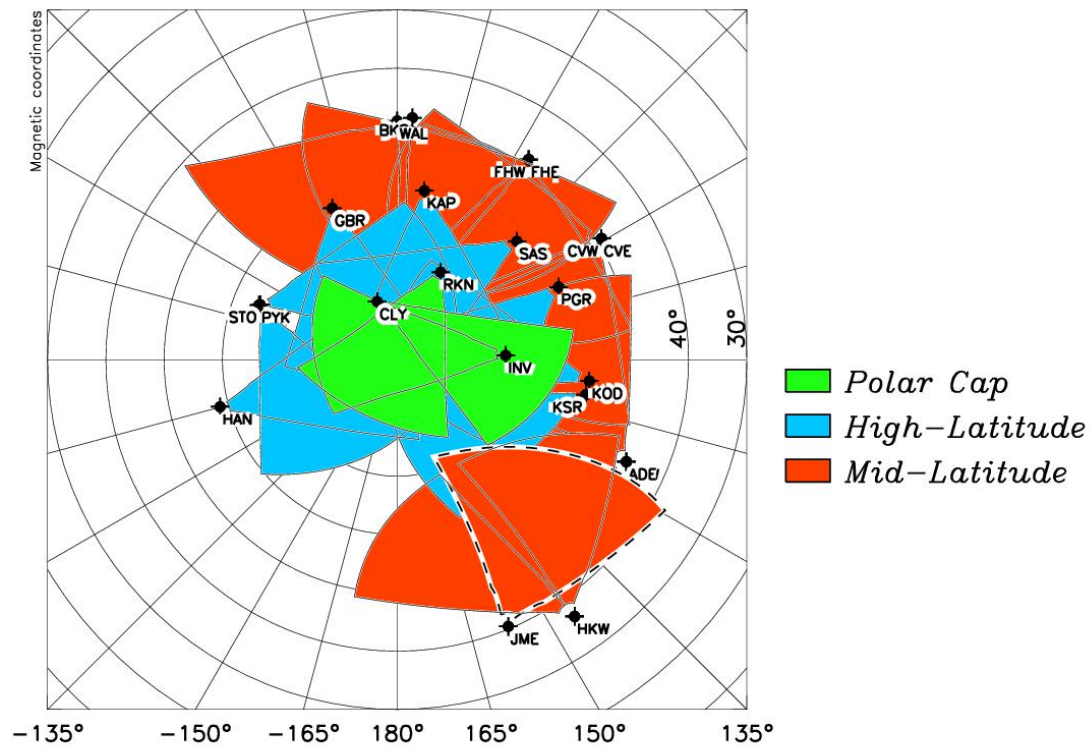


Figure 1. The fields of view of the SuperDARN radars in the Northern Hemisphere. The field of view of the Jiamusi radar is indicated by dotted lines.

2.2. Dataset and analysis

The data used in the statistical calculation were taken between March 2018 and November 2019. All beam observations were collected and analyzed, and the results with obvious or representative distribution characteristics are presented.

The numbers of days of the measurements are shown in Table 1. Each data point in the table shows the time of valid data under different seasons and Kp conditions. The difference in the time of available data in each season is related to radar commissioning or maintenance. Due to the low solar activity in 2018-2019, the number of magnetic storms is relatively low, and the data with a smaller Kp index in the statistics are dominant.

Table 1. Jiamusi radar data under different conditions

	Summer	Equinox	Winter	Total
Kp<2	2061 h	1773 h	1188 h	5022 h
2≤Kp<3	414 h	519 h	363 h	1296 h
Kp≥3	237 h	324 h	177 h	738 h
Total	2712 h	2616 h	1728 h	7056 h

Among all radar echo data, the data with a range greater than 675 km (15 range gates with 45 km per gate) from the radar are regarded as F-region scatter echoes. In the statistical process of different conditions, to eliminate possible ground and sea scatter from ionosphere scatter echoes, the data satisfying the following formula are considered ionospheric echoes: $\frac{w}{3} + |v| \leq 30\text{m/s}$.

The data with a signal-to-noise ratio less than 3 dB in the dataset are treated as nonionospheric echoes [Sundeen et al., 2004].

2.3. Total electron content

The Total Electron Content (TEC) is the total number of electrons present along a path between a radio transmitter and receiver. TEC is measured in electrons per square meter. By convention, 1 TEC Unit (TECU) = 10^{16} electrons/m². In this study, the data came from the Global Navigation Satellite System (GNSS), the original configuration is set to be a 1° × 1° geomagnetic latitude-longitude grid, and the time step is 5 minutes. The coordinate system of data is transformed from a geographic coordinate system to a geomagnetic coordinate system, and the average calculation of the long time data in each grid is carried out. Finally, the TEC distribution results under altitude adjusted corrected geomagnetic (AACGM) coordinates are obtained.

2.4. TIEGCM

The TIEGCM is a comprehensive, first-principles, three-dimensional, nonlinear representation of the coupled thermosphere and ionosphere system. It includes the dynamics, energetics, and

chemistry with a steady-state ionospheric electrodynamic in a realistic geomagnetic main field defined by the International Geomagnetic Reference Field and was developed by Dickinson et al. [1984], Roble et al. [1988], and Richmond et al. [1992]. It has 29 constant-pressure levels in the vertical coordinates, extending from approximately 97 km to 500 km in intervals of one-half scale height.

The TIEGCM uses pressure level $Z = \ln(p_0/p)$ as the vertical coordinate with the reference pressure p_0 set to $p_0=5 \times 10^7$ hPa. In the TIEGCM, the solar XUV, EUV, and FUV spectral fluxes are defined by the EUVAC model [Richards et al. 1994] using the observed F10.7 index. The high latitude energy input associated with auroral particle precipitation is calculated by an analytical auroral model. At high latitudes, the electric potential is prescribed by the empirical Weimer [2005] or Heelis et al. [1982] model. To merge the region of the wind dynamo with the high latitude region, a crossover boundary is introduced that varies dynamically with the strength of the magnetospheric forcing.

In our study, the grid spacing is 2.5° longitude and 2.5° latitude, and the time step is 10 minutes. At the same time, our inputs used average of 10.7 cm solar radio flux of 2018 (F10.7=70) and geomagnetic activity (Kp=0, 2 and 4). The altitude is set to where the pressure level $Z=2$.

3. Statistical Results

Figure 2 shows the occurrence of ionospheric echoes sorted by different seasons (summer, equinox, and winter from left to right), which is color-coded according to the color bar shown on the right. The two green lines show the distribution range of the 90-degree solar zenith angle (SZA) line in each season. The marks 0, 6, 12, and 18 in the figure represent magnetic local time. The data were collected on a grid of 12 minutes \times 1° .

Several regions of enhanced scattering occurrence rate exist in these figures. The peak rate (6%) occurs near sunset, with a slightly weaker rate at night (3-4%) and a relatively weaker rate near the dawn side and noon, except in winter. The maximum occurrence rates appeared in 20-22.5 MLT in summer, 17.5-20.5 MLT in equinox and approximately 16-17.5 MLT in winter. In winter, the peak value of the echo occurrence rate overlaps with the distribution of the SZA 90° line, while in summer and equinox, the peak value of the rate appeared slightly later than the time of the SZA 90° line. The statistical results from Ruohoniemi et al. [1988] used the data from the Goose Bay radar and also showed that a large number of echo scatter events occurred in the period when the SZA was larger than 95° . The scattering occurrence rate of this peak is approximately 5-7%, which is smaller than that derived by Hosokawa et al. [2001].

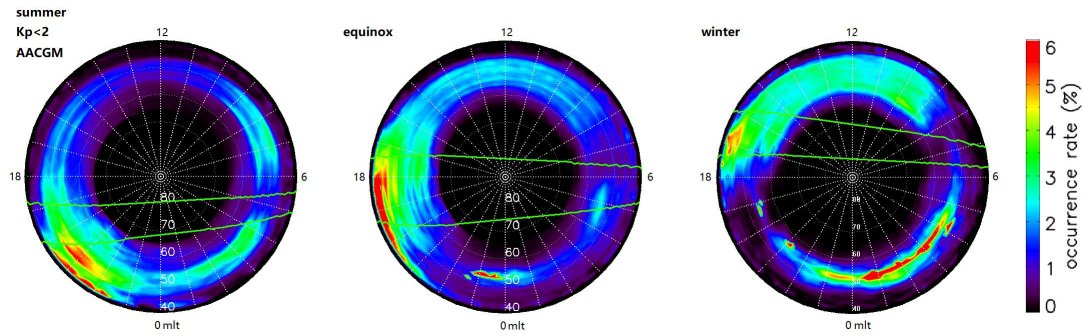


Figure 2. Distribution of the scattering occurrence rate for all Kp conditions during summer, equinox, and winter (from left to right). The results are shown in AACGM coordinates, with noon at the top and dawn at the right. The green lines show the distribution range of the SZA 90° line in the corresponding season.

Figure 3 shows the occurrence of ionospheric echoes in winter under different geomagnetic conditions. A geomagnetic activity (Kp) index less than 2 is identified as a geomagnetically quiet period (left panel); a weak disturbance period is when the Kp index is between 2 and 3 (middle panel); when the index is greater than 3 (right panel), it is considered a strong disturbance. The most obvious feature is that in the high geomagnetically active period, the occurrence rate of echoes is significantly higher than that in the quiet period. According to Jiamusi radar observation data, the range of occurrence rates greater than 6% increases as the geomagnetic index increases. Under all conditions, the occurrence rate was always relatively high on the dusk side and night side, which is similar to previous studies by Ruohoniemi et al. [1988] and Hosokama et al. [2010].

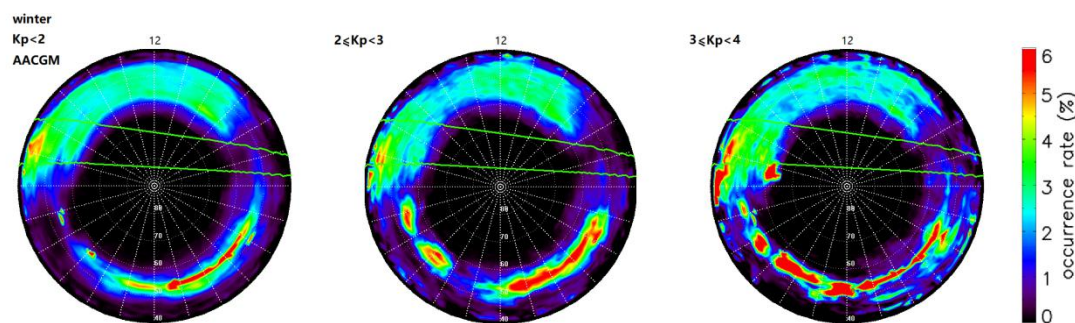


Figure 3. Distribution of the scattering occurrence rate for all seasons during different geomagnetic activities. From left to right are $K_p < 2$, $2 \leq K_p < 3$, and $K_p \geq 3$.

4. Analysis

Hosokawa et al. [2001] proposed three different interpretation models for the study of dusk scatter events using data from six Northern Hemisphere SuperDARN radars. They thought that the

sunward plasma density gradient at the sunward edge of the midlatitude trough (MIT) and an ambient electric field is a better mechanism for explaining the formation of field-aligned irregularities. Using Hokkaido East radar observation data from April 2007, Hosokawa and Nishitani calculated the ionospheric echo occurrence rate in the subauroral region. The monthly average MLT-MLAT distribution of the occurrence rate of irregularity echoes in the F region observed by the Hokkaido East radar and the empirical formula for the location of the MIT are provided. They thought that the enhancement of the dusk side occurrence rate is closely related to the sunward edge of the MIT. Liu et al. [2021] studied the formation mechanism of F-region irregularities in the midlatitude trough by using data from Swarm in situ plasma measurements. They thought that the temperature gradient drift instability was the mechanism for the formation of plasma in the MIT at night.

In this paper, the effect of the GDI on midlatitude ionospheric irregularity is discussed by the features of the distribution of TEC data and TIEGCM simulation results and the distribution of the observed occurrence rate of ionospheric F-region irregularities. In the F region, a general expression for the GDI growth rate is given by Keskinen and Ossakow [1982]:

$$\gamma^F \cong \frac{GV_E}{1 + \psi} (\vec{k} \cdot \vec{b} \times \vec{g})(\vec{k} \cdot \vec{e}),$$

where plasma drift $\vec{V}_E = \vec{E} \times \vec{B} / B^2$ and unit vectors $\vec{k} = \vec{K}/k$, $\vec{b} = \vec{B}/b$, $\vec{e} = \vec{E}/e$, and $\vec{g} = \vec{G}/g$. The wave vector \vec{K} is at which GDI waves will be generated. \vec{B} and \vec{E} are the magnetic and electric fields. The gradient values are considered relative to the background density: $G = \nabla n_0/n_0$. R is the ratio of Hall and Pedersen conductivities, and ψ is the anisotropy factor defined through $R \equiv \frac{\sigma_H}{\sigma_p} = \frac{r_i + r_e}{1 + \psi}$, i.e., $\psi = -r_e r_i$, and $r = \frac{\nu}{\Omega}$ (where ν is the collision frequency and Ω is the gyrofrequency). Generally, in the F region, $r_i \ll 1$, $r_e \ll 1$, and $\psi \ll 1$. In our paper, the distribution of $\nabla n \cdot \vec{V}_E/n$ is used as an indicator to characterize the distribution of the GDI in the F region of the midlatitude ionosphere. We chose the simulation results of the vector product of the electron density gradient and the plasma drift velocity ($\nabla n \cdot \vec{V}_E/n$) by using the TIEGCM model in the summer solstice, autumn equinox, and winter solstice to represent the GDI instability in their respective seasons.

Figure 4 shows the seasonal distributions when Kp=2 (from left to right are summer, equinox, and winter) of the TEC observed by GNSS (top), plasma drift velocity simulated by TIEGCM (middle), and the GDI indicator of $\nabla n \cdot \vec{V}_E/n$ (bottom). When the value is positive, GDI promotes the generation of irregularities; otherwise, it inhibits the generation of irregularities. It is worth noting that in the simulation, the summer solstice, autumn equinox, and winter solstice in 2018 were used to represent the plasma drift velocity distribution in summer, equinox, and winter. In the top row of Figure 4, there is always a strong electron density gradient around sunset and sunrise. At sunset, the electron density gradient points southwest, and at sunrise, it

points east or southeast. Around midnight and noon, there is a gradient of electron density toward the equator. The plasma drift velocity is dominated by the west-direction velocity most of the time, with a weak north–south component. The GDI indicator is generally positive on the dusk side and negative on the dawn side, except in winter, which has a positive value on the dawn side. The distribution of its peak value also has seasonal variation, appearing at 19.5–24 MLT in summer, 16.5–22.5 MLT in equinox, and 15–19 MLT in winter.

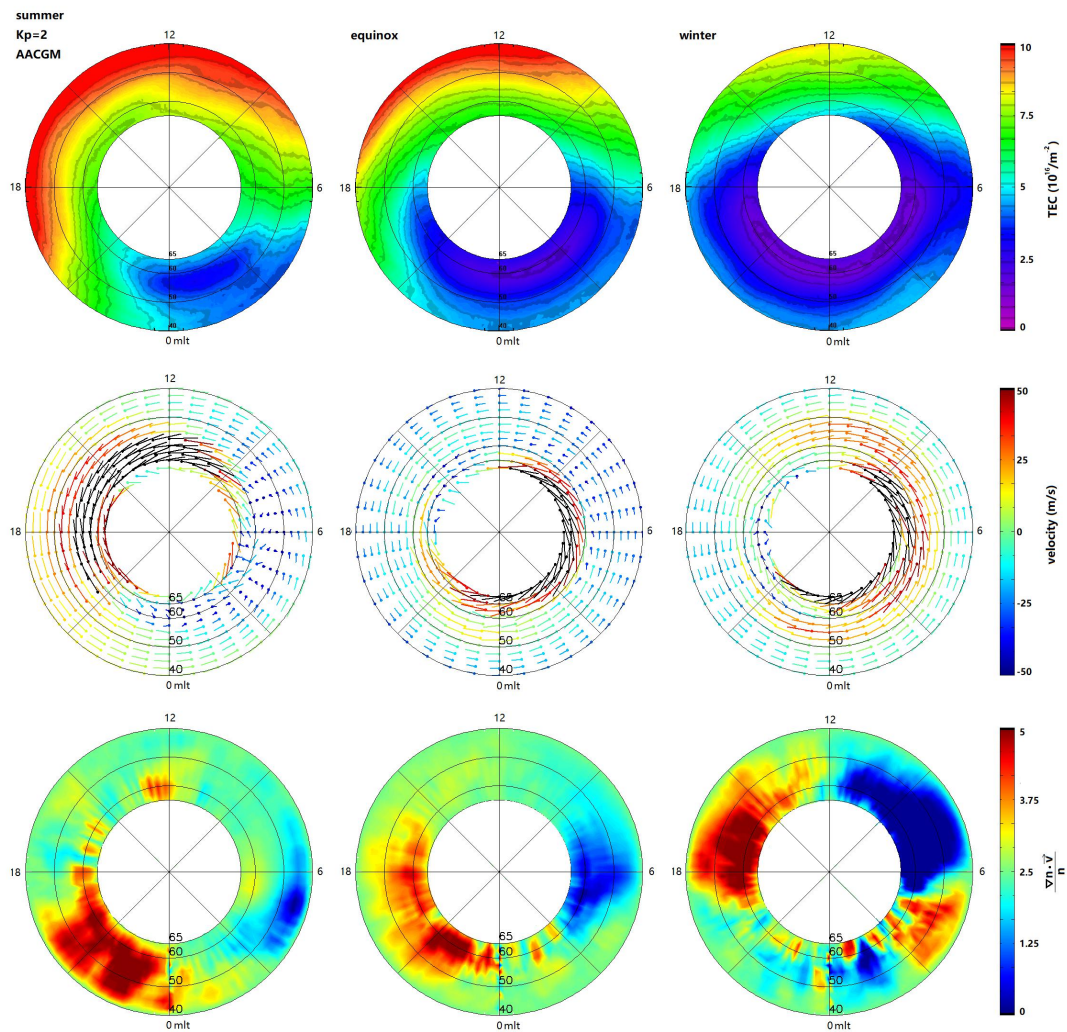


Figure 4. (top row) Distribution of TEC when Kp=2 during summer, equinox, and winter (from left to right). The plasma drift velocity (middle row) distribution in the Northern Hemisphere at a height of 300 km was obtained by the TIEGCM. The distribution of the GDI indicator of $\nabla n \cdot \vec{V}_E / n$ (bottom panel).

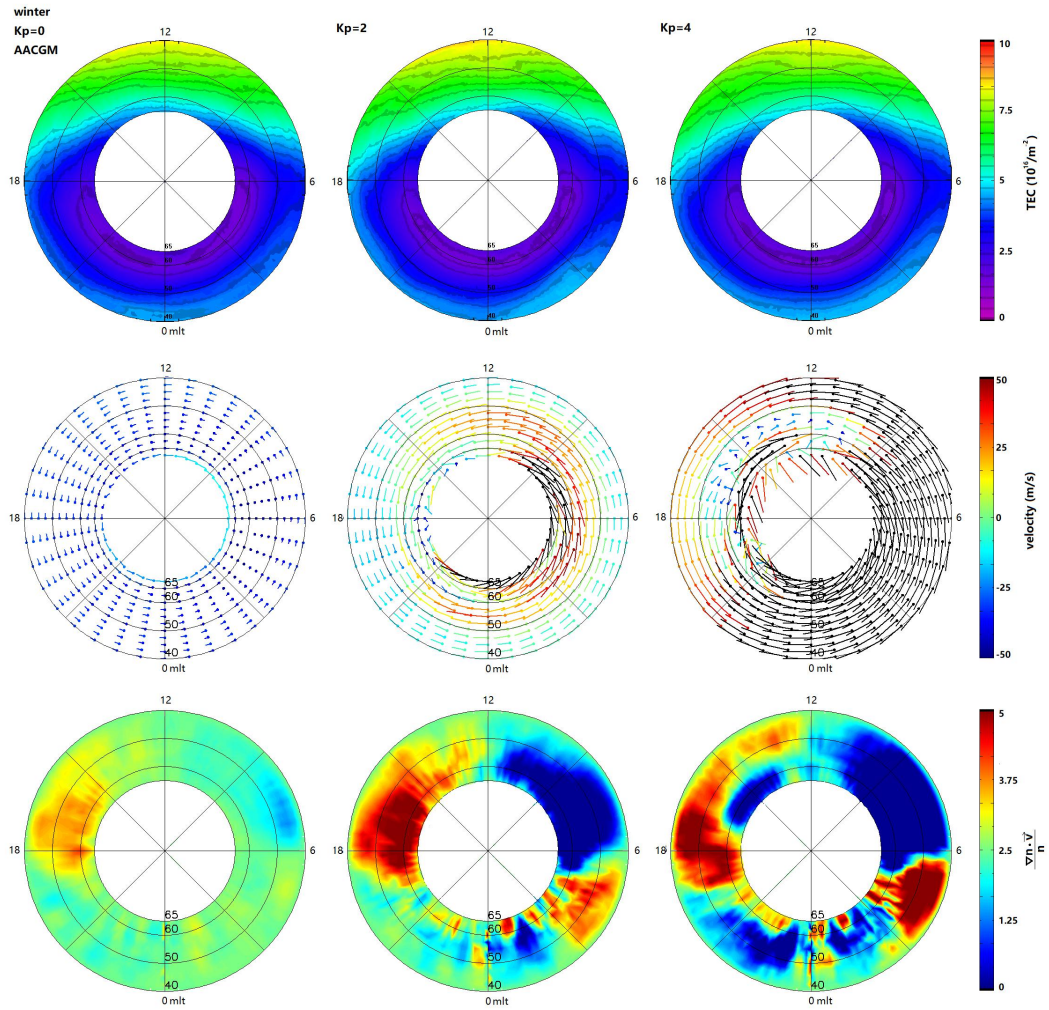


Figure 5. (top row) Distribution of TEC in summer during different geomagnetic activities (from left to right are Kp=0, 2, and 4). The plasma drift velocity (middle row) distribution in the Northern Hemisphere at a height of 300 km was obtained by the TIEGCM (winter solstice). The distribution of the GDI indicator (bottom panel).

Figure 5 shows (from top to bottom) the TECU, plasma drift velocity simulated by TIEGCM, and the GDI indicator of $\nabla n \cdot \nabla \vec{E}/n$ in winter shown in Figure 4. From left to right, the results are under the Kp=0, Kp=2, and Kp=4 conditions. Since the seasonal variation trend under different geomagnetic conditions is similar, we show the distribution of various parameters in winter as a representative. It seems that the intensity of the geomagnetic activity has little effect on the electron density distribution between 40°N-65°N MLAT in the midlatitude ionosphere in winter. However, with the increase in geomagnetic activity, the simulation results of the GDI indicator of $\nabla n \cdot \nabla \vec{E}/n$ also increase.

At sunset, the theoretical peak in the GDI is consistent with the observed distribution of irregularity. At sunrise, the GDI is relatively small and even has a negative value, which inhibits

the emergence of irregular bodies. Around midnight and noon, the GDI is relatively small and corresponds to a relatively low occurrence rate. The GDI parameters on winter nights showed negative values, contrary to the observed enhancement of echo occurrence.

5. Discussion

In the radar observation region, around sunset and sunrise, the magnetic local time distribution of the electron density gradient and the vector product of the electron density gradient and the plasma drift velocity have obvious seasonal variation. This is consistent with the echo occurrence rate variation in Figure 2. This indicates that the variation in the GDI is an important factor affecting the seasonal variation in the peak occurrence rate of radar echoes. During these two periods, the GDI is the main mechanism of ionospheric irregularity. However, at night in winter, the increase in the occurrence rate of irregularity is not consistent with the distribution of the GDI, and the increase in the occurrence rate always occurs in a narrow latitudinal range, which may indicate that the mechanism of nightside midlatitude ionospheric irregularity is no longer dominated by the GDI.

The difference at night may be related to some other factors. High latitude convective electric fields can penetrate to the middle latitudes [Senior & Blanc, 1984], which are affected by various factors, such as geomagnetic activity, interplanetary magnetic field (IMF) conditions, and ionospheric conductivity. Density fluctuations are amplified in plasma instability processes such as current-convective instability and temperature gradient instability [Raymond et al., 2006; Liu et al., 2021]. Current-convective instability occurs in regions where the field-aligned currents exceed a certain threshold, determined by the ambient parameters, and is often employed to explain the generation mechanism of field-aligned irregularities (FAIs) associated with particle precipitation and field-aligned currents. The statistical results of Liu et al. [2021] revealed that the nightside MIT region irregularities are strongly related to temperature gradient drift instability (mainly from 22 to 06 MLT).

Due to the small number of HF radars near 40°N MLAT, i.e., only the Jiamusi radar and Hokkaido radar exist, the irregularity drift velocity in this region cannot be accurately obtained by using radar data. In this paper, the GDI parameter is calculated by using the plasma drift velocity simulated by the TIEGCM. When more midlatitude radars are built in the future, a more accurate distribution function can be obtained by using the drift velocity vector in radar observations to calculate the GDI parameters.

6. Summary

We investigated the midlatitude ionospheric scattering occurrence rate by using the SuperDARN Jiamusi radar. The statistical study examined the seasonal and diurnal variations of scattering echoes and their dependence on geomagnetic activity. The findings from this analysis are as follows:

1. The Jiamusi radar scatter occurrence rate obviously depends on the magnetic local time. The echo rate on the dusk side is successively stronger than that on the night side and day side, and the occurrence rate on the dawn side is the weakest.
2. In different seasons, the maximum and minimum values of the echo occurrence rate always correspond to the location of the SZA 90° line. This phenomenon is consistent with the distribution of the GDI at that time.
3. With the increase in geomagnetic activity, the effect of the GDI increases, increasing the occurrence of irregularities.
4. GDI is not the dominant mechanism for the generation of irregularities close to midnight.

In this paper, the characteristics of the echo occurrence rate of Jiamusi radar and its correlation with seasons and geomagnetic disturbance are discussed. It is considered that the solar zenith angle affects the distribution of the peak occurrence rate. The GDI is the dominant mechanism for the occurrence of irregularities at sunset and sunrise between 40°N - 65°N MLAT. An accurate GDI distribution requires more HF radars to be built in the future to obtain a more accurate drift velocity.

Data Availability Statement

The full SuperDARN dataset is published on the Federated Research Data Repository (FRDR) (<https://www.frdr-dfdr.ca/repo/collection/superdarn>). The Kp index are available from the World Data Center for Geomagnetism, Kyoto (<http://wdc.kugi.kyoto-u.ac.jp/wdc/Sec3.html>). The TEC data are available from the CEDAR Madrigal Database (<http://cedar.openmadrigal.org>). The TIEGCM code are available from the National Center for Atmospheric Research (NCAR) (High Altitude Observatory (ucar.edu)).

Acknowledgment

This work was supported by NNSFC grants 41731070, 42174210, and 41774155, the Strategic Pioneer Program on Space Science, Chinese Academy of Sciences, Grant No. XDA15052500, and in part by the Specialized Research Fund for State Key Laboratories of China. We thank the National High-Tech Research and Development Program of China (863 program) for their support. We thank the Chinese Meridian Project for providing the Jiamusi radar data. The author J. J. Zhang was also supported by the Young Elite Scientists Sponsorship Program by the Chinese Association for Science and Technology.

References

- Blanc, M., P. Amayenc, P. Bauer, and C. Taieb, Electric field induced drifts from the French incoherent scatter facility, *Journal of Geophysical Research*, 82, 87-97, 1977.
doi: 10.1029/JA082i001p00087
- Boudouridis, A., Lyons, L. R., Zesta, E., Weygand, J. M., Ribeiro, A. J., & Ruohoniemi, J. M. (2011). Statistical study of the effect of solar wind dynamic pressure fronts on the day-side and night side ionospheric convection [Journal Article]. *Journal of Geophysical Research*, 116 (A10), 1-14. doi: 10.1029/2011JA016582
- Dickinson, R. E., E. C. Ridley, and R. G. Roble, Thermospheric general circulation with coupled dynamics and composition, *J. Atmos. Sci.*, 41, 205-219, 1984.
doi: 10.1175/1520-0469(1984)0412.0.CO;2
- Greenwald, R. A., Baker, K. B., Dudeney, J. R., Pinnock, M., Jones, T. B., Thomas, E. C., . . . Hanuise, C. (1995). Darn/SuperDARN: A global view of the dynamics of high-latitude convection. *Space Science Reviews*, 71 , 763-796. doi: 10.1007/BF00751350
- Heelis, R. A., Lowell, J. K., and Spiro, R. W.: 1982, A model of the high-latitude ionospheric convection pattern, *J. Geophys. Res.*, 87, 6339-6345 doi: 10.1029/JA087iA08p06339
- Heelis, R. A., & Coley, W.R. (1992) East-west ion drifts at mid-latitudes observed by Dynamics Explorer 2. *Journal of Geophysical Research*, 97(A12), 19,461-19,469.
doi: 10.1029/92JA01840
- Hu., H.Q., Liu, E., Liu, R., Yang, H., & Zhang, B. (2013). Statistical characteristics of ionospheric backscatter observed by SuperDARN Zhongshan radar in Antarctica. *Advances in Polar science*, 24(1), 19-31. doi: 10.3724/SPJ.1085.2013.00019
- Hosokawa, K., T. Iyemori, A.S. Yukimatu, and N. Sato (2001), Source of field-aligned irregularities in the subauroral F region as observed by the SuperDARN radars, *Journal of Geophysical Research*, 106,24,713, doi: 10.1029/2001JA900080
- Hosokawa, K. , & Nishitani, N. . (2016). Plasma irregularities in the duskside subauroral ionosphere as observed with midlatitude SuperDARN radar in Hokkaido, Japan. *Radio Science*, 45(4), -. doi: 10.1029/2009RS004244
- Keskinen, M. J., and S. L. Ossakow (1982), Nonlinear evolution of plasma enhancements in the auroral ionosphere: I. Long wavelength irregularities, *J. Geophys. Res.*, 87, 144 - 150
- Liu, Y. W., Xiong, C., Wan, X., Lai, Y. P., Wang, Y. H., Yu, X., & Ou, M. (2021). Instability mechanisms for the F-region plasma irregularities inside the mid-latitude ionospheric trough: Swarm observations. *Advancing Earth and Space Science: Space Weather*. doi:

10.1029/2021SW002785

- Maimaiti, M., Ruohoniemi, J. M., Baker, J. B. H., & Ribeiro, A. J. (2018). Statistical study of night-side quiet time mid-latitude ionospheric convection [Journal Article]. *Journal of Geophysical Research*. doi: 10.1002/2017JA024903
- Makarevich, & Roman, A. . (2015). Symmetry considerations in the two-fluid theory of the gradient drift instability in the lower ionosphere: makarevich. *Journal of Geophysical Research: Space Physics*, 119(9), 7902-7913. doi: 10.1002/2014JA020292
- Mcbride, J. B. , Ott, E. , Boris, J. P. , & Orens, J. H. . (1972). Theory and simulation of turbulent heating by the modified two-stream instability. *The Physics of Fluids*, 15(12), 1342-1347.
doi: 10.1063/1.1693881
- Oksavik, K., Greenwald, R. A., Ruohoniemi, J. M., Hairston, M. R., Paxton, L. J., Baker, J. B. H., Barnes, J. (2006). First observations of the temporal/spatial variation of the subauroral polarization stream from the SuperDARN wallops HF radar. *Geophysical Research Letters*, 31(12), 285-293. doi: 10.1029/2006GL026256
- Ossakow, S. L. . (1980). Ionospheric irregularities. *Reviews of Geophysics*, 17(1980).
doi: 10.1029/RG017i004p00521
- Robert, L, Lysak. Introduction to Space Physics[J]. *Eos, Transactions American Geophysical Union*, 1995.
- Ribeiro, A. J. , Ruohoniemi, J. M. , Baker, J. B. H. , Clausen, L. B. N. , Larquier, S. D. , & Greenwald, R. A. . (2011). A new approach for identifying ionospheric backscatter in midlatitude SuperDARN HF radar observations. *Radio Science*, 46(4), -.
doi: 10.1029/2011RS004676
- Richmond, A. D., E. C. Ridley, and R. G. Roble, A thermosphere/ionosphere general circulation model with coupled electrodynamics, *Geophys. Res. Lett.*, 6, 601-604, 1992.
doi: 10.1029/92GL00401
- Roble, R. G., R. E., Dickinson and E. C. Ridley, Seasonal and solar-cycle variations of zonal mean circulation in the thermosphere, *J. Geophys. Res.*, 82, 5493-5504, 1977.
doi: 10.1029/JA082i035p05493
- Rishbeth, H. (1971). The F-layer dynamo. *Planetary and Space Science*, 19(2), 263-267.
doi: 10.1016/0032-0633(71)90205-4
- Roth, I. , Hudson, M. K. , & Bergmann, R. . (1989). Effects of ion two-stream instability on auroral ion heating. *Journal of Geophysical Research Atmospheres*, 94(A1), 348-358.
doi: 10.1029/JA094iA01p00348

- Ruohoniemi, J. M. , Greenwald, R. A. , Villain, J. P. , Baker, K. B. , Newell, P. T. , & Meng, C. I. . (1988). Coherent hf radar backscatter from small-scale irregularities in the dusk sector of the subauroral ionosphere. *Journal of Geophysical Research Space Physics*, 93(A11), 12871-12882. doi: 10.1029/JA093iA11p12871
- Senior, C., & Blanc, M. (1984). On the control of magnetospheric convection by the spatial distribution of ionospheric conductivities. *Journal of Geophysical Research*, 89 (A1), 261-284. doi: 10.1029/JA089iA01p00261
- Sundeen, S., Blanchard, G., & Baker, K. (2004). Reanalysis of criteria for identifying ground scatter. In: SuperDARN 2004 Workshop, Saskatoon, Canada.
- Thomas, E., Baker, J., Ruohoniemi, J. M., Hosokawa, K., Erickson, P. J., Coster, A. J., & Foster, J. C. (2014). An examination of the source of decameter-scale irregularities in the geomagnetically disturbed mid-latitude ionosphere. 2014 United States National Committee of URSI National Radio Science Meeting (USNC-URSI NRSM). IEEE. doi:0.1109/USNC-URSI-NRSM.2014.6928078
- Wang, W, Zhang, J.J., Wang, C., Nishitani, N., Yan, J.Y., Lan, A.L., Deng, X., & Qiu, H.B. (2021). Statistical Characteristics of mid-latitude Ionospheric Irregularities at Geomagnetic Quiet Time: Observations from the Jiamusi and Hokkaido East SuperDARN HF Radars. *Journal of Geophysical Research*, doi: 10.1029/2021JA029502
- Weimer, D. R.: 2005, Improved ionospheric electrodynamic model and application to calculating Joule heating rates. *J. Geophys. Res.*, 110, A05306. doi: 10.1029/2004ja010884
- Yang, T. Y., Kwak, Y. S., Kil, H., Lee, Y. S., Lee, W. K., & Lee, J. J. (2015). Occurrence climatology of F region field-aligned irregularities in middle latitudes as observed by a 40.8mhz coherent scatter radar in Daejeon, South Korea. *Journal of Geophysical Research*, 120 (11), 10107-10115. doi: 10.1002/2015JA021885
- Zhang, J. J., Wang, W., Wang, C., Lan, A. L., Yan, J. Y., Xiang, D., Shi, X. (2020). First observation of ionospheric convection from the Jiamusi HF radar during a strong geomagnetic storm. *Earth and Space Science*, 7 (1). doi: 10.1029/2019EA000911